Measurement-induced entanglement transitions in the quantum Ising chain: From infinite to zero clicks

Xhek Turkeshi [1,2,3,*] Alberto Biella [4,5,3] Rosario Fazio,[2,6] Marcello Dalmonte [1,2] and Marco Schiró[3]

[1]*SISSA, via Bonomea 265, 34136 Trieste, Italy*
[2]*The Abdus Salam International Centre for Theoretical Physics (ICTP), Strada Costiera 11, 34151 Trieste, Italy*
[3]*JEIP, USR 3573 CNRS, Collège de France, PSL Research University, 11 Place Marcelin Berthelot, 75321 Paris Cedex 05, France*
[4]*Université Paris-Saclay, CNRS, LPTMS, 91405 Orsay, France*
[5]*INO-CNR BEC Center and Dipartimento di Fisica, Università di Trento, 38123 Povo, Italy*
[6]*Dipartimento di Fisica, Universitá di Napoli "Federico II," Monte S. Angelo, I-80126 Napoli, Italy*

We investigate measurement-induced phase transitions in the quantum Ising chain coupled to a monitoring environment. We compare two different limits of the measurement problem: the stochastic quantum-state diffusion protocol corresponding to infinite small jumps per unit of time and the no-click limit, corresponding to postselection and described by a non-Hermitian Hamiltonian. In both cases we find a remarkably similar phenomenology as the measurement strength γ is increased, namely, a sharp transition from a critical phase with logarithmic scaling of the entanglement to an area-law phase, which occurs at the same value of the measurement rate in the two protocols. An effective central charge, extracted from the logarithmic scaling of the entanglement, vanishes continuously at the common transition point, although with different critical behavior possibly suggesting different universality classes for the two protocols. We interpret the central charge mismatch near the transition in terms of noise-induced disentanglement, as suggested by the entanglement statistics which displays emergent bimodality upon approaching the critical point. The non-Hermitian Hamiltonian and its associated subradiance spectral transition provide a natural framework to understand both the extended critical phase, emerging here for a model which lacks any continuous symmetry, and the entanglement transition into the area law.

I. INTRODUCTION

Recent years have seen major progress in the understanding of many-body quantum dynamics. Two well separated limits have been discussed extensively: the unitary dynamics of closed isolated systems [1,2] and the dissipative dynamics of open quantum systems coupled to an external environment [3]. In the former case the system remains in a pure many-body state which, in the absence of ergodicity breaking [4,5], acts as an efficient bath for any of its subsystems, leading to thermalization of local observables and volume-law entanglement entropy. In the latter, the system is intrinsically mixed and described by a master equation for the density matrix. The competition between unitary and dissipative couplings in this setting can lead to nonequilibrium phase transitions but it is not expected to change the entanglement properties of the system.

An intermediate situation which has recently attracted major attention is the one in which the external environment represents a measurement apparatus, which ceaselessly probes some property of the system. Here the key physics is encoded in stochastic quantum many-body trajectories, which contain a much richer information on the system dynamics than the average state. As a result, new dynamical

phases arise, which are characterized by different entanglement properties. For generic unitary evolution, as that encoded in random circuits [6–36], these systems show a transition between an error correcting phase and a Zeno phase, signaled by the transition of entanglement from a volume to an area law.

If instead the unitary dynamics is generated by a Hamiltonian, the properties of the system depend on the nature of the latter [37–41]. For instance, in the case of a free fermion Hamiltonian, the volume law is unstable for any measurement rate to a subextensive entanglement content [42,43]. However, it has been shown that the average entanglement entropy can still show a transition between a logarithmic and area law phase at a critical measurement strength or to display a purely logarithmic scaling, depending on the stochastic protocol [44]. A logarithmic growth of the entanglement entropy in an entire phase is particularly intriguing, given that the average state is expected to be effectively thermal, and it is reminiscent of a critical, conformally invariant phase whose origin has been so far elusive. Similar results have been obtained for free-fermion random circuits with temporal randomness [45], a setting that has been recently generalized to higher dimension [46], or for Majorana random circuits [47,48].

A different take on measurement-induced transitions has instead focused on the limit of postselection, also called forced measurement phase transitions [16], where only

*xturkesh@sissa.it

atypical trajectories with a particular outcome of measurement are retained. In this regime several works have discussed the relationship between measurement-induced transitions and the spectral properties of the associated non-Hermitian Hamiltonian [49–51]. More recently a non-Hermitian Hamiltonian has been also shown to emerge from the replica field theory associated to monitored Luttinger liquids, leading to a Kosterlitz-Thouless transition between a gapless and a gapped phase [52].

In light of these developments it is interesting to compare the entanglement properties of stochastic quantum dynamics and non-Hermitian Hamiltonian, in a simple and paradigmatic setting. With such motivation, in this work we consider the one-dimensional quantum Ising model coupled to an environment which continuously measures its transverse magnetization. Specifically, we focus on two rather opposite limits of the measurement problem: the quantum state diffusion protocol [53,54], a very clear, experimentally realizable measurement protocol in quantum optical systems [55], equivalent to homodyne trajectories [56,57], and the quantum jump protocol in the so-called no-click limit, corresponding to a purely deterministic non-Hermitian evolution, which amounts to postselecting only trajectories without jumps.

Remarkably, despite describing rather different limits, these protocols show a very similar phenomenology in their entanglement properties. In particular, upon increasing the ratio γ between measurement rate and Hamiltonian coupling we find in both protocols a transition from a critical phase to an area law phase, the former characterized by a logarithmic scaling of the entanglement with time and system size. Right at the transition point γ_c, which we find numerically to coincide in the two protocols, the prefactor of the logarithmic entanglement contribution, interpreted as an effective central charge, vanishes continuously.

We note that an extended phase with logarithmic (critical) scaling of the entanglement was found also for other free-fermionic systems under monitoring, for example, the XX chain of Ref. [44]. Yet this result occurs here for a model, the quantum Ising chain, which does not conserve particle number but only its parity, and thus lacks any obvious continuous symmetry expected in conventional gapless systems. This suggests that the role of microscopic symmetries in the classification of quantum phases of matter, leading to the textbook distinction between gapped and gapless phases in the presence of discrete/continuous symmetries, needs to be revisited for quantum many-body systems under monitoring, as recently pointed out [48].

In this respect the no-click limit offers a natural explanation both for the critical entanglement scaling and for its transition towards an area law: these can be naturally understood by looking at the spectral properties of the non-Hermitian quantum Ising chain which undergoes, right at γ_c, a subradiance transition from an extended critical phase with gapless decay modes, to a gapped phase which is smoothly connected to the dark state of the measurement operator.

In spite of the important similarities, the two protocols differ for the behavior of the effective central charge as a function of the measurement rate. In particular, we find this quantity to be larger in the no-click limit, a signature
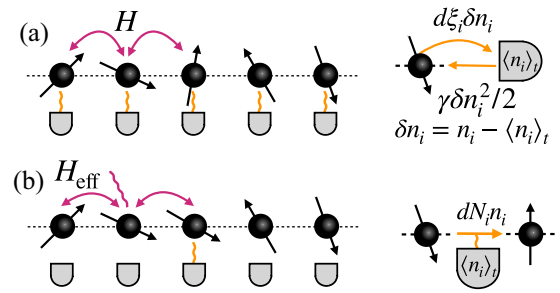

FIG. 1. Cartoon of the monitored quantum Ising chain. (a) Quantum state diffusion protocol: on each lattice site a two-level system (Ising spin) interacts with its neighbors and is subject to a weak-continuous measurement of the up-polarized state. (b) Quantum jump protocol: the spins in the chain interact through a non-Hermitian Hamiltonian. Occasionally a quantum jump takes place, projecting the measured degree of freedom in the up-polarized state. The no-click limit corresponds to postselecting only trajectories without jumps (see text for details).

of a noise-induced disentangling effect that appears clearly in the statistics of the entanglement entropy, which shows emergent bimodality upon approaching the critical point. Our results highlight the key role played by the non-Hermitian Hamiltonian for the qualitative understanding of entanglement transitions and suggest that different stochastic ensembles provide different universality classes of a common critical phenomenon.

The paper is structured as follows. In Sec. II we introduce the model and the measurement protocols. Then we discuss the results for the two protocols in Sec. III, in particular the entanglement dynamics (Sec. III A), the entanglement scaling with system size (Sec. III B), and the entanglement statistics (Sec. III C). We detail in the Appendices a derivation of the protocol of interest, and a summary of the numerical methods used for the simulations.

II. MODEL AND MEASUREMENT PROTOCOLS

We consider a one-dimensional quantum Ising chain with Hamiltonian

$$H = J \sum_{i=1}^{L-1} \sigma_i^x \sigma_{i+1}^x \tag{1}$$

with open boundary conditions, evolving under the competing effect of its own unitary dynamics and the measurement of the up-polarized state $n_i \equiv (\sigma_i^z + 1)/2 = |1\rangle\langle 1|$ (pictorially illustrated in Fig. 1). Here σ^α are the Pauli matrices. We now introduce the two measurement protocols that will be considered in this work, namely. the quantum state diffusion and the quantum jumps with postselection, corresponding to the non-Hermitian Hamiltonian.

A. Stochastic quantum dynamics with continuous monitoring

Due to the monitoring, the evolution is captured by quantum trajectories $|\psi(\boldsymbol{\xi}_t)\rangle$ which follow the quantum state

diffusion (QSD) equation

$$d|\psi(\boldsymbol{\xi}_t)\rangle = -iHdt|\psi(\boldsymbol{\xi}_t)\rangle + \sum_{i=1}^{L}(n_i - \langle n_i\rangle_t)d\xi_t^i|\psi(\boldsymbol{\xi}_t)\rangle$$

$$- \frac{\gamma}{2}\sum_{i=1}^{L}(n_i - \langle n_i\rangle_t)^2 dt|\psi(\boldsymbol{\xi}_t)\rangle \qquad (2)$$

(see Appendix A for a brief derivation of the above stochastic Schrödinger equation). The first term in Eq. (2) represents the unitary evolution, while the remaining encode the noise effects. The $d\xi_t^i$ are Îto increments of a Wiener process $\boldsymbol{\xi}_t = (\xi_t^1, \xi_t^2, \dots, \xi_t^L)$, responsible for the stochastic nature of the trajectories, with zero mean $\overline{d\xi_t^i} = 0$ and fulfilling the exact property $d\xi_t^i d\xi_t^j = \gamma dt\delta^{ij}$. The last term in Eq. (2) describes a deterministic back action from the measuring environment.

We note the presence of a feedback mechanism in Eq. (2), as the noise contributions couple to the fluctuations of the measured operator $\delta n_i = n_i - \langle n_i\rangle_t$ where $\langle \circ \rangle_t = \langle\psi(\boldsymbol{\xi}_t)| \circ |\psi(\boldsymbol{\xi}_t)\rangle_t$ is the average over the quantum state. The role of this feedback is to preserve the norm of the state (and any of its cumulant) for any realization of the noise.

It is important to stress the difference between the conditional and the mean state [42]. The conditional state is the quantum trajectory itself $\rho_t(\boldsymbol{\xi}_t) = |\psi(\boldsymbol{\xi}_t)\rangle\langle\psi(\boldsymbol{\xi})_t|$, fixed by a realization of the Wiener process. Instead, the mean state is given by

$$\overline{\rho_t} = \int \mathcal{D}\boldsymbol{\xi}_t P(\boldsymbol{\xi}_t)|\psi(\boldsymbol{\xi}_t)\rangle\langle\psi(\boldsymbol{\xi}_t)| \qquad (3)$$

with $P(\boldsymbol{\xi}_t)$ the probability distribution of the noise. Despite that the conditional state is always pure, the mean state is mixed, and follows the Lindblad master equation

$$\frac{d}{dt}\overline{\rho_t} = -i[H, \overline{\rho_t}] - \frac{\gamma}{2}\sum_i[n_i, [n_i, \overline{\rho_t}]]. \qquad (4)$$

This difference is crucial, and highlights how the two states $\overline{\rho_t}$ and $\rho_t(\boldsymbol{\xi}_t)$ provide rather different information on the statistical properties of the system. For observables which are linear in the state $O[\rho] = O\rho$, due to the linearity of the disorder average, the mean state $\overline{\rho_t}$ encodes the statistical properties of O. Specifically, for any function $f(O)$, we have

$$\overline{\text{tr}[\rho_t(\boldsymbol{\xi}_t)f(O)]} \equiv \text{tr}[f(O)\overline{\rho_t}]. \qquad (5)$$

However, the above relationship fails if one is interested in the noise average of quantities which depend *nonlinearly* on the density matrix. A simple example involves the purity $\mathcal{P}(\rho) = \text{tr}\rho^2$: while for the conditional state $\mathcal{P}[\rho_t(\boldsymbol{\xi}_t)] = 1$ (and hence its disorder average), for the mean state we have $\mathcal{P}(\overline{\rho_t}) < 1$. In general, similar issues arise when one is interested in a more subtle statistical correlation of the stochastic process, for example, in the so-called overlaps $\overline{O_i(t)O_j(t)} = \overline{\langle O_i\rangle_t \langle O_j\rangle_t}$. We emphasize that this situation is essentially analogous to the difference between annealed and quenched averages in disordered systems [58].

After this parenthesis, we introduce the main observable of interest: the (von Neumann) entanglement entropy [59–62]. Given a partition $A \cup B$, the (conditional) reduced density matrix $\rho_A(\boldsymbol{\xi}_t) = \text{tr}_B\rho(\boldsymbol{\xi}_t)$ encodes the bipartite entanglement.

The entanglement entropy is defined as

$$S(\boldsymbol{\xi}_t) = -\text{tr}_A[\rho_A(\boldsymbol{\xi}_t) \ln \rho_A(\boldsymbol{\xi}_t)]. \qquad (6)$$

We note that this is a well defined measure of entanglement provided that the overall state is pure, in which case it yields the amount of Bell pairs that can be distilled from the quantum state. This is not the case for an overall mixed state, such as the averaged state in Eq. (3), where also classical correlation enters into this quantity [63]. For this reason, throughout the paper we only consider the conditional state and the conditional average of the entanglement entropy. To simplify the notation, we furthermore omit the conditional specification. After evolving the state under Eq. (2), we compute the entanglement entropy. Its average is given by

$$\overline{S} = \int \mathcal{D}\boldsymbol{\xi}_t P(\boldsymbol{\xi}_t)S(\boldsymbol{\xi}_t), \qquad (7)$$

as well as its full probability distribution is

$$P(S_t) = \int \mathcal{D}\boldsymbol{\xi}_t P(\boldsymbol{\xi}_t)\delta[S - S(\boldsymbol{\xi}_t)]. \qquad (8)$$

Throughout this paper we set $J = 1$ and study the problem by varying the strength of the measurement γ and for different system sizes L.

B. Non-Hermitian Hamiltonian

When the measurements act occasionally but abruptly on the quantum state, the quantum trajectories are described by the following stochastic Schrödinger equation:

$$d|\psi(\boldsymbol{N}_t)\rangle = -iHdt|\psi(\boldsymbol{N}_t)\rangle - \frac{\gamma}{2}dt\sum_i(n_i - \langle n_i\rangle_t)|\psi(\boldsymbol{N}_t)\rangle$$

$$+ \sum_i\left(\frac{n_i}{\sqrt{\langle n_i\rangle_t}} - 1\right)\delta N_t^i|\psi(\boldsymbol{N}_t)\rangle, \qquad (9)$$

where $\boldsymbol{N}_t$ is a Poisson process, with $\delta N_t^i = 0, 1, (\delta N_t^i)^2 = \delta N_t^i$, and $\overline{\delta N_t^i} = \gamma dt\langle n_i\rangle_t$. [A derivation of Eq. (9) is given in Appendix A.] The dynamics generated by Eq. (9) preserves the purity of the state for each trajectory, and gives an alternative unravelling of the average dynamics in Eq. (4).

When $\delta N_t^i = 0$ on every site, the evolution is driven by the non-Hermitian Hamiltonian

$$H_{\text{eff}} = J\sum_{i=1}^{L-1}\sigma_i^x\sigma_{i+1}^x - i\frac{\gamma}{2}\sum_{i=1}^{L}n_i, \qquad (10)$$

while when any $\delta N_t^i = 1$, the last term in Eq. (9) dominates and projects the measured degree of freedom onto the up-polarized state $|1\rangle_i$. The feedback constant $\propto i\gamma\sum_i\langle n_i\rangle_t$ enters as a renormalization of the wave function within the non-Hermitian evolution driven by Eq. (10). In the following we consider a postselection of the stochastic dynamics, which arises when, among the experimental runs, we select a portion of trajectories where measurements do not take place (no-click limit). The evolution is therefore deterministic, and driven by the non-Hermitian Hamiltonian in Eq. (10). In particular, the effect of the environment enters the imaginary part of Eq. (10). Here we notice that this limit captures different aspects of the weak measurement-induced dynamics

compared to the quantum state diffusion. In the framework of quantum jumps, the latter arise in the limit of infinite measurement events, and hence correspond to an infinite-click dynamics [64].

The dynamics of this non-Hermitian Hamiltonian has been considered previously in Ref. [49], where a subradiant transition has been observed in relationship to a quantum-Zeno effect. Here we study its entanglement properties, namely, we evolve the initial density matrix $\rho_0 = |00\ldots0\rangle\langle00\ldots0|$ according to

$$\rho(t) = \frac{e^{-iH_{\text{eff}}^{\dagger}t}\rho_0 e^{iH_{\text{eff}}t}}{\text{Tr}\left(\rho_0 e^{iH_{\text{eff}}t}e^{-iH_{\text{eff}}^{\dagger}t}\right)}, \tag{11}$$

where the denominator takes into account the term proportional to $\gamma\,dt\sum_i\langle n_i\rangle_t$ in Eq. (9). Then, given a partition $A \cup B$, we construct the reduced density matrix $\rho_A(t) = \text{tr}_B\rho(t)$ which encodes the bipartite entanglement. As stressed before, the non-Hermitian Hamiltonian provides a deterministic protocol, hence the entanglement entropy is deterministic:

$$S(t) = -\text{tr}_A[\rho_A(t)\ln\rho_A(t)]. \tag{12}$$

To explore the stationary regime, in order to avoid residual dynamical oscillations, we consider

$$S(\infty) \equiv \lim_{t\to\infty}\frac{1}{t - t_{\text{sat}}}\int_{t_{\text{sat}}}^t ds\, S(s). \tag{13}$$

As for the monitoring case, we make use of the Jordan-Wigner mapping to write down the non-Hermitian Ising model in Eq. (10) in terms of a quadratic fermionic model (see Appendix B).

III. RESULTS

In this section we present the results of the numerical simulations for the quantum state diffusion and the non-Hermitian Hamiltonian. After a discussion of the entanglement growth within both paradigms, we compare the entanglement scaling at the stationary state. Finally, we investigate the entanglement statistics of the quantum state diffusion protocol, and relate it to the non-Hermitian results.

A. Entanglement growth

We start considering the initial state $|\psi_0\rangle = |00\ldots0\rangle$ and evolve the system according to the QSD protocol defined in Eq. (2). This setup is suitable to investigate the entanglement generation in the system, as the initial state has zero entanglement being a product state. (We have checked, but not presented here, that our results are robust against a different choice of initial product state.) We make use of the Jordan-Wigner mapping to write the monitored Ising model as a quadratic model of spinless fermions, which can be solved efficiently. (Details on the free fermion techniques, and on the numerical implementation are given in Appendix B). For the computation of entanglement, we choose a subsystem A of L_A contiguous sites. The average entanglement evolution is shown in Fig. 2. For small to intermediate values of γ [see panels (a)–(c)] we find a logarithmic growth in time of
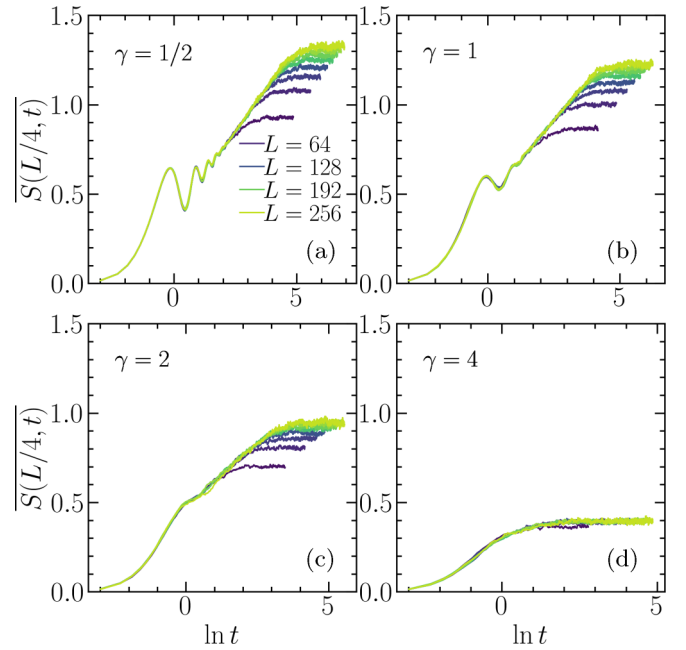

FIG. 2. Dynamics of the entanglement entropy averaged over $N = 2000$ trajectories for different values of the measurement strength γ, different system sizes L, and fixing $L_A = L/4$. (a)–(c) We see a logarithmic growth in time of the entanglement (note the logarithmic scale for the time axis) with a saturation to a size-dependent plateau, for $\gamma < 4$ and a much slower growth to a value independent from system size, for $\gamma > 4$.

the entanglement,

$$\overline{S(t)} \sim \ln t, \tag{14}$$

which ultimately saturates at times $t_{\text{sat}} \sim L/\gamma$. It is worth emphasizing that already a small monitoring rate γ is enough to give rise to a nontrivial entanglement dynamics compared to the isolated system oscillation (generated by $H = \sum_i \sigma_i^x \sigma_{i+1}^x$). In other words the interplay between measurements and unitary evolution can increase the entanglement production, at least in a certain region of the parameters, as also noted in Ref. [49]. However, upon further increasing the measurement rate we see a substantial change of the entanglement growth which already for $\gamma = 4$ shows a rapid saturation to a plateau that is almost independent from the size, a trend that continues for larger values of γ.

The results of the entanglement dynamics for the non-Hermitian Ising model [cf. Eq. (12)] are given in Fig. 3. For small values of γ [panels (a)–(c)], we see that the entropy exhibits an overall logarithmic growth, which resembles the result for the QSD protocol, but has the important difference of exhibiting residual oscillations which dress both the growth and the saturation regimes. Upon further increasing the measuring strength γ the entanglement dynamics in the non-Hermitian case displays a sharp transition towards a regime characterized by a fast approach to a stationary value, with no oscillations. Our numerics locate the boundary between these dynamical regimes around $\gamma \sim 4$, an estimate compatible with what was found for the QSD protocol. As we will discuss in the next section, we can understand the origin
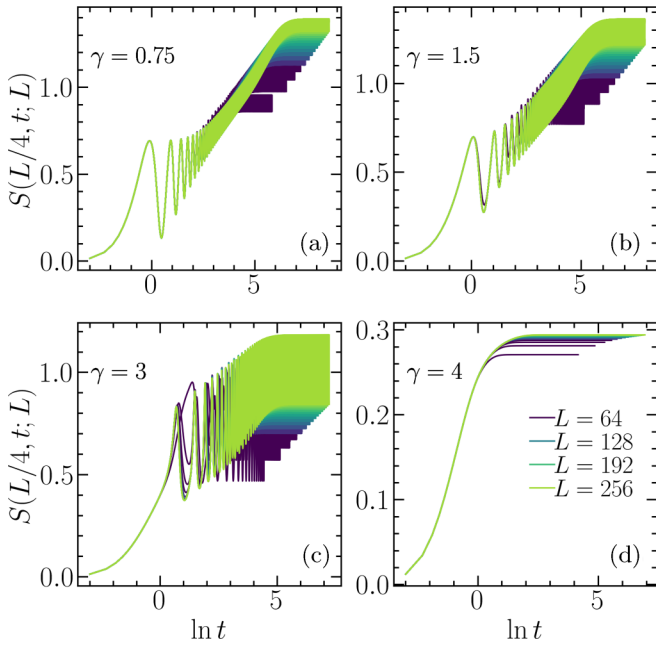
FIG. 3. Entanglement dynamics for the non-Hermitian Hamiltonian for different values of the measurement rate γ and different system sizes. For small γ [panel (a)] we see a logarithmic growth in time and a saturation to a plateau that depends on system sizes. For large γ [panel (b)] the entanglement rapidly saturates to a value that does not depend on size. Approaching the transition point we see strong oscillations in the dynamics.

of this sharp transition by looking at the spectral properties of the non-Hermitian Hamiltonian.

B. Entanglement scaling and effective central charge

As we have seen, at long enough times the entanglement reaches a stationary value in both protocols. We first discuss the scaling of this stationary entanglement with system size. This usually provides key insights on the properties of the system at long times. To this extent we chose a subsystem of $L_A = L/4$ contiguous spins and plot in Fig. 4 the long-time entanglement as a function of L and different values of γ.

For the quantum state diffusion protocol, we can clearly distinguish a regime of logarithmic entanglement growth with system size for small γ, which eventually evolves into a much weaker dependence, an almost constant plateau for large measurement rates [see Fig. 4(a)]. As we are going to discuss further below, those two regimes are separated by a sharp entanglement transition.

We note that a logarithmic scaling of the average entanglement in an extended region of parameters is a particularly intriguing result which was obtained before in free-fermion models with a continuous $U(1)$ symmetry [44] and more recently in connection with a Berezinskii-Kosterlitz-Thouless (BKT) transition [48,52]. Here we find this result for a model which only features a discrete Z_2 symmetry and whose ground state would show logarithmic scaling of the entanglement only at the critical point. This suggests that a different mechanism, not directly related to the microscopic symmetries of the
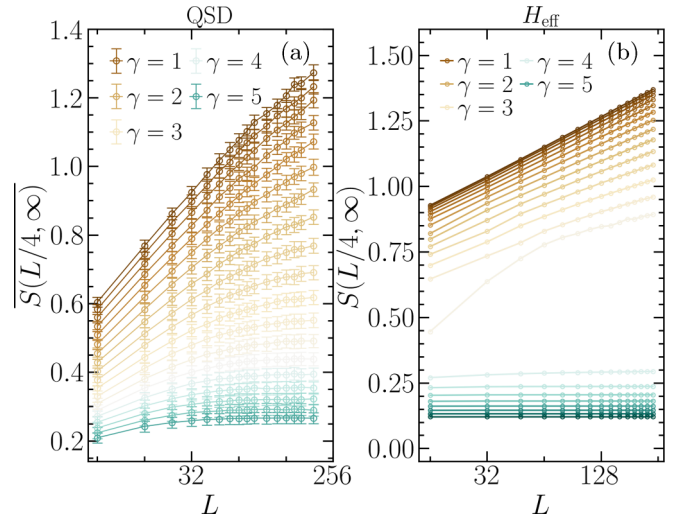

FIG. 4. Stationary-state entanglement entropy as a function of the length of the chain. (a) Average entanglement entropy for the QSD protocol. (b) Long-time entanglement entropy for the non-Hermitian dynamics. In both cases we see a transition from a logarithmic *critical* scaling, for small γ to an area law (constant) scaling at large γ. Different curves in the two panels correspond to increasing values of γ, from $\gamma = 0.25$ (top curve) to $\gamma = 6$ (bottom curve) with a $\Delta\gamma = 0.25$.

problem, could be behind the origin of this seemingly *critical* phase.

Interestingly, the finite-size scaling of the entanglement entropy for the non-Hermitian Hamiltonian shows a behavior which is qualitatively similar to the QSD protocol, as we show in Fig. 4(b), including a logarithmic scaling for small γ and an area-law (constant) scaling for large measurement rates, separated by a sharp transition. We also note that the two scaling regimes are connected by a finite-size crossover, absent in the stochastic QSD protocol, whose characteristic scale we found to diverge at the transition (not shown).

For equilibrium quantum critical systems the prefactor of the logarithmic scaling of the entanglement entropy is controlled by the central charge of the associated conformal field theory(CFT) [59], a universal quantity which roughly measures the number of degrees of freedom in the CFT. Following this analogy, Ref. [44] introduced an *effective central charge* for an XX spin chain under continuous monitoring, which turned out to be a nonuniversal function of the measurement rate. Here we follow this route and define an effective central charge for both the QSD protocol and the non-Hermitian Hamiltonian by fitting the data in Fig. 4 according to the ansatz

$$\text{QSD} \quad \overline{S} = \tfrac{1}{3}c_{\text{QSD}}(\gamma)\ln L + a,$$
$$H_{\text{eff}} \quad S = \tfrac{1}{3}c_{H_{\text{eff}}}(\gamma)\ln L + b. \qquad (15)$$

Here a and b are two system-size independent quantities.

We plot the result in Fig. 5 and find that $c(\gamma)$ decreases with γ and, quite remarkably, vanishes for both protocols around the same value of measurement strength $\gamma_c \simeq 4$, that we therefore establish as critical value for the entanglement transitions between logarithmic and area-law regimes. Our
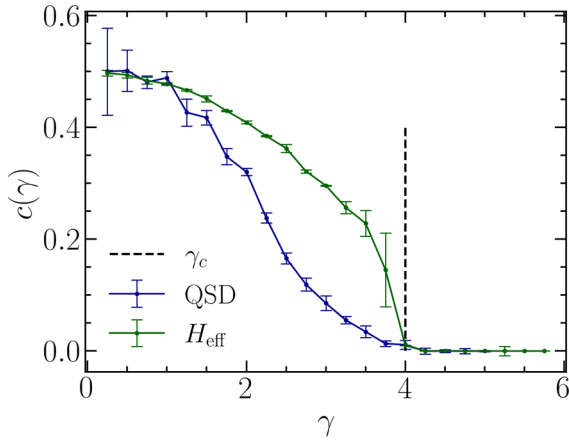
FIG. 5. Effective central charge as a function of the measurement rate γ, for the QSD protocol and the non-Hermitian dynamics. In both cases we find that $c(\gamma)$ decreases monotonously and vanishes around $\gamma_c \simeq 4$, which locates the entanglement transition between logarithmic scaling and area law. Interestingly the two central charges coincide at small and large values of γ, while approaching the critical point we find the non-Hermitian one to be larger, possibly vanishing at γ_c in a nonanalytic way.

results are consistent with the unbiased fit on the region $\gamma > 4$, which, for the investigated values, is compatible with zero within errorbar. Despite this similarity we notice that the effective central charge shows a rather different dependence from γ in the QSD and in the non-Hermitian Hamiltonian protocols. In particular, a direct comparison in Fig. 5 shows that the effective central charges coincide at small and large values of γ, while they deviate in a region before the critical point. Here the non-Hermitian effective central charge turns out to be larger than the one associated to the QSD protocol, a point on which we will come back to in the next section.

Before closing this section we note that many of the properties found for the entanglement dynamics of the non-Hermitian Hamiltonian can be naturally understood in terms of the spectral properties of the non-Hermitian Ising model in Eq. (10). In fact this can be easily diagonalized once written in fermionic language [49,65,66], and takes the form

$$H_{\mathrm{eff}} = \sum_{k>0} \Lambda_k (\bar{\eta}_k \eta_k + \eta_{-k} \bar{\eta}_{-k}) + E_0, \qquad (16)$$

where $\bar{\eta}_k, \eta_k$ are fermionic operators obtained from a non-Hermitian Bogolyubov rotation, E_0 is an additive constant fixing the energy zero, and Λ_k are the quasiparticle energies. We note that these are in general complex, as the model lacks any $\mathcal{PT}$ symmetry and read

$$\Lambda_k = 2\sqrt{1 - \frac{\gamma^2}{16} + i \frac{\gamma}{2} \cos k}. \qquad (17)$$

The non-Hermitian Ising model features a subradiance transition at a critical value of the measurement rate, given exactly by $\gamma_c = 4$, at which the state with smallest imaginary part changes in a nonanalytic way [49]. For small $\gamma < \gamma_c$ the imaginary part of the spectrum in Eq. (17) is *gapless* and, consistently, the correlation functions in this phase decay as a power law [66], a result which is at odds with a model possessing only a discrete symmetry. From this point of view

the logarithmic scaling of the entanglement entropy can be naturally understood, since the entire phase $\gamma < \gamma_c$ has soft modes with small quasidegenerate lifetime, which are responsible for the slow growth of the entanglement. On the other hand, the real part of the spectrum is gapped for $\gamma < \gamma_c$, leading to residual oscillations in the entanglement dynamics.

Above the subradiance transition for $\gamma > \gamma_c$ a gap opens up in the imaginary part of the spectrum Λ_k, which is consistent with the fast entanglement dynamics found in this regime. The correlation functions in this phase are expected to decay exponentially over a length diverging as $\gamma \to \gamma_c^+$, a fact that can naturally explain the emergence of a crossover in the finite-size entanglement scaling. We note that in the subradiant phase the long-time dynamics is controlled by a pair of states with the smallest nonzero imaginary part. These in the strong measurement limit coincide with the dark states of the measurement operator, which are factorized (uncorrelated) eigenstates of the transverse magnetization, therefore justifying the small, system-size independent entanglement entropy.

We note that the non-Hermitian protocol can be also easily generalized to an Ising model evolving in the presence of a real transverse field h, in addition to the imaginary one due to the measurement rate. In this case we expect, from the analysis of the quasiparticle spectrum, that a spectral and entanglement transition would occur at a field-dependent rate $\gamma_c(h)$. A complete analysis of the dynamics in this case is, however, beyond the scope of this work and left for future works.

Finally, the insights on the non-Hermitian Hamiltonian could suggest that an effective field theory description could be possible for $\gamma < \gamma_c$ and that the effective central charge could be computed using field theory replica techniques [67], which, however, we do not attempt here. We also note that, in this perspective, an effective central charge which depends on a parameter in a nonuniversal way seems very natural, and in fact several nonunitary field theories have been shown to enjoy this property [45,68,69].

C. Entanglement statistics

Additional insights are given by the statistical fluctuations of the entanglement in the quantum state diffusion protocol, a feature that goes beyond the simple average so far discussed and that is encoded in the full probability distribution, $P(S_t)$, defined in Eq. (8). Concretely, we investigate this distribution at stationarity and evaluate $P(S_\infty) = \lim_{t \to \infty} P(S_t)$.

As we see in Fig. 6, the statistics of entanglement shows a rather rich evolution with γ. In particular, we see that in the logarithmic phase ($\gamma < \gamma_c$), the statistics changes dramatically, much more than what one could have guessed from the average value, whose dependence from γ can be reabsorbed in a renormalization of the central charge. For small values of the measurement rate, $\gamma \lesssim 1$ [panel (a)], the entanglement distribution is a normal Gaussian which broadens asymmetrically for $\gamma \sim 2$ [panel (b)] and develops an emergent bimodality as the critical point γ_c is approached [panels (c)–(e)]. Specifically we see that already for $\gamma = 2.75$ a secondary peak, for lower values of the entanglement, starts to emerge. Upon further increasing γ we see a transfer of weight between the high-entanglement and low-entanglement peaks, with the latter ultimately becoming the dominant one as the system
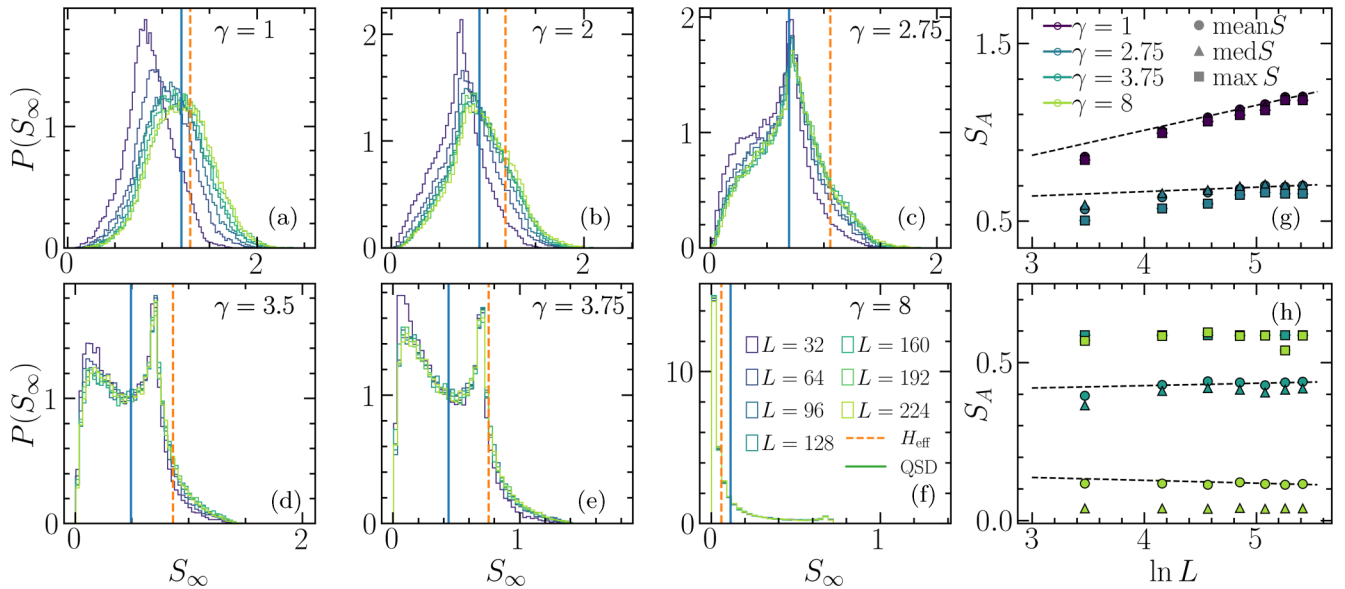
FIG. 6. (a)–(f) Probability distribution of the entanglement entropy for different values of γ and different system sizes. The realization collected for these functions is $N = 64\,000$. We see that upon increasing γ, the statistic evolves from a simple Gaussian [panels (a) and (b)] to a skewed distribution [panels (c)–(e)], with emergent bimodality. At large γ, the distribution is peaked at $S_\infty \simeq 0$ [panel (f)]. The solid line shows the average (blue line) over the trajectories for the quantum state diffusion, and the stationary value of the non-Hermitian Hamiltonian (orange line). (g),(h) Different statistical estimators $\langle\langle S \rangle\rangle$ versus system size for different values of γ. Note the logarithmic scaling in the L axis.

enters the area-law phase. Here, for $\gamma > \gamma_c$ the entanglement distribution is strongly skewed and peaked around small values of the entropy.

It is interesting to discuss the size dependence of the histograms, which is rather different depending on the value of γ. In particular, as we show in Fig. 6(g), where we plot the average, median, and typical entanglement for different L and γ, we find that for $\gamma \lesssim 2.5$ all indicators scale logarithmically with L. Instead, Fig. 6(h) shows that approaching the critical point ($\gamma = 3.75$) and above it ($\gamma = 8$) the statistical estimators deviate from each other, a signature of the non-Gaussianity of the entanglement distribution. In the area-law phase for $\gamma > \gamma_c$ the scaling of all the statistical proxies considered becomes independent on the system size.

The emergence of bimodality in the entanglement statistics is an interesting result, which suggests that within the log phase the entanglement is not a self-averaging quantity, and that limiting the discussion to the average value could hide important features of the problem. A similar result was found in the monitored XX model under QSD protocol [44] and, in Ref. [49] for the statistics of the return probability and the local transverse magnetization under a quantum jump stochastic protocol. In this latter case it was shown that the non-Hermitian Hamiltonian captured a secondary peak in the distribution of the relevant observables.

It is therefore interesting to compare the statistical properties of the entanglement in the QSD protocol with the non-Hermitian Hamiltonian. This comparison is proposed in Fig. 6, where we indicate with a dashed line the long-time entanglement in the non-Hermitian case and with a blue line the average entanglement of the QSD protocol. We see that indeed the non-Hermitian Hamiltonian provides a good proxy for the average entanglement both for small γ, when

entanglement fluctuations are Gaussian, as well as for large γ when the statistics is dominated by small values of the entanglement entropy. For intermediate values of γ instead, when the statistics becomes strongly bimodal and fluctuations due to the noise are more relevant, the entanglement content of the non-Hermitian Hamiltonian is systematically larger than the average, reflecting the atypical nature of the no-click process. This is not surprising in retrospect, as the QSD protocol contains randomness which is expected to decrease the entanglement content of the system as opposed to the translational-invariant non-Hermitian protocol. We note also that in addition to the leading scaling behavior of the entanglement, captured by the effective central charge, there is also a nonuniversal correction to the entanglement that depends in principle on γ and could play a role in the precise comparison between the two protocols.

IV. CONCLUSION

In this work we have discussed measurement-induced criticality in a quantum Ising chain coupled to a monitoring environment. We have focused on two different limits of the measurement problem, corresponding respectively to the quantum state diffusion protocol and the no-click dynamics, the latter described by a non-Hermitian Ising model.

In both cases we found a sharp phase transition in the entanglement properties of the system, as a function of the measurement rate γ. The entanglement dynamics out of an initial product state evolves from a slow logarithmic growth at small measurement rates to a fast approach to a stationary value at large γ. The stationary-state entanglement shows a *critical* logarithmic scaling with respect to system size, with an effective central charge which changes continuously with

γ and vanishes at a critical strength γ_c, indicating a transition towards an area-law scaling which we found numerically to coincide in the two protocols. The existence of an extended critical phase with logarithmic scaling of the average entanglement is particularly surprising for our Ising model which, differently from others stochastic measurement problems considered recently in the literature, lacks a continuous symmetry usually associated with gapless critical behavior. The no-click limit and associated non-Hermitian evolution provides a natural mechanism for this phenomenology, in terms of a spectral (subradiant) phase transition from a critical phase with gapless decay modes at small measurements to a gapped area-law phase. We also find important differences between the two protocols, in particular in the behavior of the effective central charge as a function of the measurement strength which turns out to be larger in the non-Hermitian case. This effect, which seems to suggest different universality classes depending on the specific measurement ensemble, can be understood in terms of a disentangling effect of the noise.

APPENDIX A: CONTINUOUS MEASUREMENTS AND STOCHASTIC SCHRÖDINGER EQUATIONS

This Appendix is an overview of stochastic quantum dynamics in the Hilbert space (see Refs. [54,64,70,71] for a general review). We first introduce the positive-operator value measurements (POVM), which arise naturally when system and environment interact for a finite time. In the limit of weak measurement, the system evolves through a stochastic Schrödinger equation, the details of which depend on the environment specifics. We consider two possible choices of system-environment setups which naturally translate, respectively, in the quantum state diffusion Eq. (2) and in the quantum jump equation (9). From the latter, the non-Hermitian quantum Hamiltonian equation (10) is obtained through postselection. These equations correspond to different unravelling of the same master equation, highlighting the independence of the mean state Eq. (3) from the stochastic protocols.

1. Weak measurements and quantum trajectories

Measurement lies at the core of quantum mechanics. Given a state $|\psi\rangle$, and an observable O, the von Neumann postulates states that, when a measurement takes place, the wave function collapses in the eigenvector $|n\rangle$ of O corresponding to the measurement outcome o_n. This can be seen as the transformation

$$|\psi\rangle \mapsto |\psi'\rangle = \frac{P_n|\psi\rangle}{\|P_n|\psi\rangle\|}. \tag{A1}$$

Here $P_n = |n\rangle\langle n|$ is the projector to the eigenspace of o_n (the observable is resolved as $O = \sum_n o_n P_n$), and $p_n \equiv \langle\psi|P_n|\psi\rangle$ is the measurement probability.

These projective measurements are an idealization: they are implicitly instantaneous, and they collapse a pure state into a pure state. In contrast, real-world experiments are imperfect: they require a finite time of interaction with the system, and in general the outcome state is mixed. Positive-operator value measurements represent a generalization of projective measurements, which are suitable to treat situations where the interaction time between system and ancilla is comparable to the energy scale of the system.

Given a set of positive operators E_n which sum to the identity $\sum_n E_n = 1$, it is possible to define the probabilities $p_n = \text{tr}(\rho E_n)$. Differently from the projective case, these operators are not orthogonal, hence the knowledge of E_n does not fix the state after the measurement. It is necessary to know a set of operators $A_{n,k}$ such that $E_n = \sum_k A_{nk}^\dagger A_{nk}$ (dubbed Kraus operators). Then, the state after the measurement outcome corresponding to E_n is

$$\rho \mapsto \rho' = \frac{\sum_k A_{nk}\rho A_{nk}^\dagger}{\text{tr}(\rho E_n)}. \tag{A2}$$

It is clear that in general, given a pure density matrix ρ, the outcome measurement in Eq. (A2) is mixed. The condition to preserve purity is that $E_n = A_n^\dagger A_n$, i.e., there is only one Kraus operator per measurement. In this case Eq. (A2) can be recast in a wave-function perspective

$$|\psi\rangle \mapsto |\psi'\rangle = \frac{A_n|\psi\rangle}{\sqrt{\langle\psi|E_n|\psi\rangle}}. \tag{A3}$$

POVM can be implemented by allowing the system to interact with an ancilla for a finite time, and apply afterward a projective measurement to the ancilla. The limit when this interaction is small is the weak measurement, when typically the state of the system is mildly perturbed.

As an example, we consider the toy model of a two-level system $|\psi\rangle = \sum_{n=0,1} c_n^S|n\rangle_S$ which interacts with a two-level ancilla initialized in a state $|a\rangle = \sum_{k=0,1} c_k^A|k\rangle_A$. If their interaction is infinitesimal, the unitary evolution of the combined system initialized in $|\Psi\rangle = |\psi\rangle \otimes |a\rangle$ is given by

$$U(\epsilon) = \exp\left[-i\epsilon \sum_j O_j^S \otimes O_j^A\right]. \tag{A4}$$

After the unitary transformation, entanglement is generated, and the state up to first order in ϵ is given by

$$|\Psi'\rangle(\epsilon) = \sum_{m,n} \left(c_n^S c_m^A - i\epsilon c_{nm}^{\text{ent}}\right)|n\rangle_S \otimes |m\rangle_A,$$

$$c_{nm}^{\text{ent}} = \sum_j \sum_{n',m'=0,1} O_{j,n',n}^S O_{j,m',m}^A c_{n'}^S c_{m'}^A, \tag{A5}$$

$$O_{j,k,k'}^\mu \equiv \langle k|O^\mu|k'\rangle_\mu, \quad \mu = S, A.$$

Rearranging the above equation, the system is given by

$$|\Psi'\rangle(\epsilon) = \alpha(\epsilon)|\phi_0\rangle_S \otimes |0\rangle_A + \beta(\epsilon)|\phi_1\rangle_S \otimes |1\rangle_A, \quad \text{(A6)}$$

where the constants α, β, and ϕ_k are read out matching Eqs. (A5) and (A6). If a measurement is now performed on the ancilla along the z direction, one obtains

$$|\psi\rangle = \begin{cases} |\phi_0\rangle, & \text{with probability} \quad p_0 = |\alpha(\epsilon)|^2, \\ |\phi_1\rangle, & \text{with probability} \quad p_1 = |\beta(\epsilon)|^2. \end{cases} \quad \text{(A7)}$$

Hence, POVM can be implemented by carefully designing the system-ancilla interaction, the ancilla initial state, and the projective measurement on the ancilla. To conclude, let us notice that, in the case of the two-level ancilla, the Kraus operators are one for each measurement type. Hence, the measurements are generated by $E_k = A_k^\dagger A_k$, $k = 0, 1$. This is a convenient, but not unique, setting to guarantee the purity preservation of the state. Furthermore, as stressed, the precise form of the operators A_k depends on the microphysics of the system and ancilla. As we shall see, to derive a stochastic Schrödinger equation it is usually necessary to expand up to second order in the parameter ϵ. (Nonetheless, the above argument is still valid.) In the following we shall assume that the Kraus operators (and hence the POVM) are given by the problem, thus simplifying the discussion.

2. Quantum state diffusion

We consider the following Kraus operators:

$$A_0 = \sqrt{\tfrac{1}{2}}|0\rangle\langle 0| + \sqrt{\tfrac{1}{2} - \epsilon}|1\rangle\langle 1|, \quad \text{(A8)}$$

$$A_1 = \sqrt{\tfrac{1}{2}}|0\rangle\langle 0| + \sqrt{\tfrac{1}{2} + \epsilon}|1\rangle\langle 1|. \quad \text{(A9)}$$

Starting from the state $|\psi\rangle = \alpha|0\rangle + \beta|1\rangle$, after the measurement the state is in one of the following two states:

$$|\phi_0\rangle = \frac{A_0|\psi\rangle}{\sqrt{p_0}} = \alpha\left(|\beta|^2\epsilon + \frac{3}{2}|\beta|^4\epsilon^2\right)|0\rangle$$
$$+ \beta\left(\epsilon(1 - |\beta|^2) + \frac{\epsilon^2}{2}(-1 - 2|\beta|^2 + 3|\beta|^4)\right)|1\rangle, \quad \text{(A10)}$$

$$|\phi_1\rangle = \frac{A_1|\psi\rangle}{\sqrt{p_1}} = \alpha\left(-|\beta|^2\epsilon + \frac{3}{2}|\beta|^4\epsilon^2\right)|0\rangle$$
$$+ \beta\left(-\epsilon(1 - |\beta|^2) + \frac{\epsilon^2}{2}(-1 - 2|\beta|^2 + 3|\beta|^4)\right)|1\rangle, \quad \text{(A11)}$$

with probability respectively $p_0 = 1/2 - |\beta|^2\epsilon$ and $p_1 = 1/2 + |\beta|^2\epsilon$. The above postmeasurement state can be collected into a compact differential form, by introducing the random binomial variable $dW = \mp\epsilon$, and the operator $n = |1\rangle\langle 1|$. We have

$$d|\psi\rangle = |\psi'\rangle - |\psi\rangle = 2\epsilon^2(\langle n\rangle^2 - 2\langle n\rangle n)|\psi\rangle$$
$$+ dW(n - \langle n\rangle)|\psi\rangle - \frac{\epsilon^2}{2}(n - \langle n\rangle)^2|\psi\rangle, \quad \text{(A12)}$$

where $\langle \circ \rangle = \langle \psi| \circ |\psi\rangle$ is the state average. The expression can be simplified by centering the random variable $dW \mapsto$

$d\xi = dW - \overline{dW}$, since the average $\overline{dW} = 2\beta^2\epsilon^2 = 2\langle L\rangle\epsilon^2$ due to the $\mathcal{O}(\epsilon)$ unbalance in the outcome probability. The variance is preserved at leading order $d\xi^2 = \epsilon = dW^2$, and the equation reads

$$d|\psi\rangle = d\xi(n - \langle n\rangle)|\psi\rangle - \frac{\epsilon^2}{2}(n - \langle n\rangle)^2|\psi\rangle. \quad \text{(A13)}$$

Equation (A13) gives one interaction with a single ancilla qubit. In order to derive a stochastic Schrödinger equation we subsequently couple a series of identically prepared ancillas with the same paradigm. Hence, Eq. (A13) is iterated multiple times. Taking the scaling limit, with infinitesimal time step we have

$$\frac{d|\psi(\xi_t)\rangle}{dt} = \frac{d\xi_t}{dt}(n - \langle n\rangle_t)|\psi(\xi_t)\rangle - \frac{\epsilon^2}{2dt}(n - \langle n\rangle_t)^2|\psi(\xi_t)\rangle. \quad \text{(A14)}$$

Fixing the scaling $\epsilon^2 = \gamma dt$ reduces this equation to

$$d|\psi(\xi_t)\rangle = d\xi_t(n - \langle n\rangle_t)|\psi(\xi_t)\rangle - \frac{\gamma}{2}dt(n - \langle n\rangle_t)^2|\psi(\xi_t)\rangle. \quad \text{(A15)}$$

This is the quantum state diffusion equation for a two-level qubit.

Let us make some final comments. (i) The scaling $\epsilon = \sqrt{\gamma dt}$ is typical when dealing with Kraus operators (for instance, see Refs. [3,54,64] for an in-depth discussion). This is due to a Markovian approximation, which is assumed to hold for the systems of interest. (ii) The generalization to multiple qubits is trivial. Recovering the noise terms in Eq. (2) requires the introduction of L uncorrelated Îto terms $d\xi_i$ with $\overline{d\xi} = 0$ and $d\xi_i d\xi_j = \gamma dt \delta_{ij}$. (iii) For the time evolution in the limit $dt \to 0$, the binomial variable can be approximated by a Gaussian increment, in the same spirit as obtaining a Wiener process from a random walk.

3. Quantum jumps and non-Hermitian Hamiltonian

We consider the following Kraus operators:

$$A_0 = |0\rangle\langle 0| + \cos\epsilon|1\rangle\langle 1|, \quad \text{(A16)}$$
$$A_1 = \sin\epsilon|1\rangle\langle 1|. \quad \text{(A17)}$$

In this situation, given the state $|\psi\rangle = \alpha|0\rangle + \beta|1\rangle$, the measurements E_0 and E_1 are unbalanced, with probability $p_0 = 1 - |\beta|^2\epsilon^2$ and $p_1 = |\beta|^2\epsilon^2$, respectively. As in the previous section, we introduce the operator $n = |1\rangle\langle 1|$. The state after the measurement is in either of the following states:

$$|\phi_0\rangle = |\psi\rangle + \tfrac{1}{2}\alpha\langle n\rangle\epsilon^2|0\rangle + \tfrac{1}{2}\beta(\langle n\rangle - 1)\epsilon^2|1\rangle$$
$$= |\psi\rangle - \tfrac{1}{2}(n - \langle n\rangle)\epsilon^2|\psi, \quad \text{(A18)}$$
$$|\phi_1\rangle = |1\rangle. \quad \text{(A19)}$$

In differential form, we have

$$d|\psi\rangle = -\frac{1}{2}(n - \langle n\rangle)\epsilon^2|\psi\rangle + \left(\frac{n}{\sqrt{\langle n\rangle}} - 1\right)\delta N|\psi\rangle. \quad \text{(A20)}$$

Here δN is a Poisson process: $\delta N = 0(1)$ with probability $p_0(p_1)$. Since $\overline{\delta N} = |\beta|^2\epsilon^2$, the state is unlikely to experience

a measurement and usually is affected only by the Kraus operator A_0. However, when $\delta N = 1$, the second term in Eq. (A20) dominates the infinitesimal one, and projects the state onto $|1\rangle$. Notice that in this case $\delta N^2 = \delta N$.

Suppose that the system interacts with n ancilla qubits. As previously discussed, the stochastic Schrödinger equation is given once the scaling $\epsilon^2 = \gamma dt$ is set:

$$d|\psi(N_t)\rangle = -\frac{1}{2}(n - \langle n\rangle_t)\gamma dt|\psi(N_t)\rangle$$
$$+ \left(\frac{n}{\sqrt{\langle n\rangle_t}} - 1\right)\delta N_t|\psi(N_t)\rangle. \quad (A21)$$

This is the so-called quantum jump equation. The first term is a non-Hermitian Hamiltonian, while the second term is the quantum jump. When the event happens, the state is projected to $|1\rangle\langle 1|$. It is interesting to ask how much is the probability that the state does never jump? The probability of this no-click dynamics for one qubit is given by

$$P_{\text{no-click}} = \Pi_{n=0}^{\infty} p_0 \simeq |\alpha|^2. \quad (A22)$$

Thus, the number of trajectories with no-jump effect is substantial.

We conclude with a few remarks. (i) The generalization to many body is trivial, once L uncorrelated variables are included, and the Hamiltonian H of the system is added. The final equation for the quantum jumps is Eq. (9). The non-Hermitian Hamiltonian in Eq. (10) is recast when postselecting the trajectories without jumps. Notice that the contribution $\propto \gamma dt \sum_i \langle n_i\rangle_t$ factorizes as an overall rescaling of the wave function, and cancels out in the average. (ii) In the situation of a spin chain, the probability of no-click dynamics (hence non-Hermitian generated dynamics) depends on the system size. In practice, one chooses among all the trajectories the portion where no jump has occurred. This postselection process is key in investigating non-Hermitian physics in experimental setups. (ii) Both the quantum jump and the quantum state diffusion equations induce the same Lindblad evolution Eq. (4) for the mean state. This difference highlights how quantum trajectories contain substantially more information than the average state. Importantly, the non-Hermitian Hamiltonian coincides with the noncoherent term of the Lindblad equation (4).

APPENDIX B: FREE-FERMION TECHNIQUES AND NUMERICAL IMPLEMENTATION

In this Appendix we present a summary of the simulation techniques used in this paper. (For a general reference on the ideas used here, see Ref. [72].) These methods are based on the fermionic representation of the Ising model, which can be applied also to Eq. (2) [Eq. (10)], as the noise (non-Hermitian) term preserves the quadratic structure. We first review the Jordan-Wigner transformation, and explain how the time evolution reads in fermionic variables. Due to the Gaussian preservation of both quantum state diffusion and non-Hermitian Hamiltonian, the state is fully characterized by its two-point function. Afterwards, we show how the entanglement entropy is derived from the correlation matrix. Finally, we give some detail of the numerical implementation.

1. Jordan-Wigner mapping

The Jordan-Wigner transformation is defined by

$$\sigma_i^x = K_i(c_i + c_i^\dagger), \quad K_i = \prod_{j<i}(2n_i - 1), \quad (B1)$$

$$n_i = c_i^\dagger c_i. \quad (B2)$$

Here, the string operator K_i ensures the fermionic algebra. For the quantum state diffusion Eq. (2), the dynamics maps to

$$d|\psi(\boldsymbol{\xi}_t)\rangle = -i\sum_{i=1}^{L-1}(c_i^\dagger c_{i+1} + c_i^\dagger c_{i+1}^\dagger + \text{H.c.})dt|\psi(\boldsymbol{\xi}_t)\rangle$$
$$+ \sum_{i=1}^{L}(n_i - \langle n_i\rangle_t)d\xi_t^i|\psi(\boldsymbol{\xi}_t)\rangle$$
$$- \frac{\gamma}{2}dt\sum_{i=1}^{L}(n_i - \langle n_i\rangle_t)^2|\psi(\boldsymbol{\xi}_t)\rangle. \quad (B3)$$

Instead for the non-Hermitian Hamiltonian Eq. (10), we have

$$d|\psi\rangle = -i\sum_{i=1}^{L-1}(c_i^\dagger c_{i+1} + c_i^\dagger c_{i+1}^\dagger + \text{H.c.})dt|\psi\rangle$$
$$- \frac{\gamma}{2}dt\sum_{i=1}^{L}n_i|\psi\rangle. \quad (B4)$$

Within this formalism, if the initial state of the system is Gaussian, then the state is Gaussian at each time step. In particular, all the observables are encoded in the correlation matrix

$$G_{ij} = \begin{pmatrix} \langle c_i^\dagger c_j\rangle & \langle c_i^\dagger c_j^\dagger\rangle \\ \langle c_i c_j\rangle & \langle c_i c_j^\dagger\rangle \end{pmatrix}. \quad (B5)$$

In the next section, we show how the dynamics can be reduced to the time evolution of a $2L \times 2L$ matrix.

2. Dynamics in the fermionic formalism

The equation of motion for both the protocols can be written as $d|\psi(\boldsymbol{\xi}_t)\rangle = dZ_t|\psi(\boldsymbol{\xi}_t)\rangle$, where dZ_t is quadratic in the creation/destruction fields. For the quantum state diffusion

$$dZ_t = dt\left(-iH - \frac{\gamma}{2}\sum_i(n_i - \langle n_i\rangle_t)^2\right)$$
$$+ \sum_i d\xi_t^i(n_i - \langle n_i\rangle_t), \quad (B6)$$

while for the non-Hermitian Hamiltonian we have

$$dZ_t = dt\left(-iH - \frac{\gamma}{2}\sum_i n_i\right) = -idtH_{\text{eff}}. \quad (B7)$$

Both these instances can be treated on the same footing, once the operator dZ_t is specified. From the operator dZ_t, it is possible to write down an equation of motion for the correlation matrix Eq. (B5). [This is obtained by taking the differential of Eq. (B5), simplifying the fermionic algebra, and expanding up to order $O(dt)$].

However, in practical implementation, this method is not the most efficient. A better strategy, which we follow in this paper, is the route pioneered in Ref. [42]. Since the system is Gaussian, for any t, there exists a unitary matrix

$$\mathcal{U}_t = \begin{pmatrix} U_t & V_t^\dagger \\ V_t & U_t^\dagger \end{pmatrix} \qquad (B8)$$

such that

$$|\psi\rangle_t = \frac{1}{\sqrt{|\det U_t|}} \exp\left(-\frac{1}{2} \sum_{i,j,k} (U_t)_{i,k} (V_t^\dagger)_{k,j} c_i^\dagger c_j^\dagger \right) |0\rangle. \qquad (B9)$$

This condition is equivalent to finding a unitary transformation that maps the original fermionic fields $(c_i, c_j^\dagger)$ to a new set $(\chi_i, \chi_j^\dagger)$ such that $\chi_i |\psi\rangle_t = 0$ for all i. Explicitly, labeling a vector of fermionic field as $\mathbf{c} = (c_1, c_2, \ldots, c_L)$,

$$\begin{pmatrix} \chi \\ \chi^\dagger \end{pmatrix} = \mathcal{U}_t \begin{pmatrix} \mathbf{c} \\ \mathbf{c}^\dagger \end{pmatrix}. \qquad (B10)$$

From the definition of the correlation matrix and Eq. (B9), and after few manipulations in fermionic algebra, we have the relationship

$$G(t) = \mathcal{U}_t \begin{pmatrix} \mathbf{1}_{L\times L} & \mathbf{0}_{L\times L} \\ \mathbf{0}_{L\times L} & \mathbf{0}_{L\times L} \end{pmatrix} \mathcal{U}_t^\dagger. \qquad (B11)$$

Hence, the full evolution is encoded in $\mathcal{U}_t$. The equation of motion for this object are easily derived from Eq. (B10) and using the annihilation condition $\chi_i |\psi\rangle_t = 0$. In practice it can be implemented into two steps. (i) Integrate the Heisenberg equation of motion between t and $t + dt$ (with initial condition $\mathcal{U}_{t=0} = \mathcal{U}_0$ given):

$$d\mathcal{U}_t = 2 d\mathcal{Z}_t \mathcal{U}_t. \qquad (B12)$$

(ii) Apply a renormalization to guarantee that U_{t+dt} is unitary (for instance, a QR decomposition). This guarantees that $|\psi\rangle_{t+dt}$ is in the form Eq. (B9) with the operators given in U_{t+dt}. For concrete details on the numerical implementation, see Appendix B 4.

3. Majorana fermions and entanglement entropy

For a Gaussian state, Wick's theorem reduces the computation of entanglement from diagonalizing a $2^L \times 2^L$ matrix to a $2L \times 2L$ linear problem. For this goal, it is convenient to

introduce two species of Majorana fermions:

$$a_{j,1} = c_j + c_j^\dagger, \quad a_{j,2} = i(c_j^\dagger - c_j). \qquad (B13)$$

Then the matrix

$$V = \begin{pmatrix} \mathbf{1}_{L\times L} & \mathbf{1}_{L\times L} \\ -i\mathbf{1}_{L\times L} & i\mathbf{1}_{L\times L} \end{pmatrix} \qquad (B14)$$

transforms the correlation function from Dirac fermions to Majorana $W = VGV^\dagger$. Due to the Majorana algebra $\{a_{i,p}, a_{j,q}\} = \delta_{i,j}\delta_{p,q}$, the Majorana correlation can be decomposed into $W = \mathbf{1} + i\tilde{W}$. The matrix $\tilde{W}$ is real and antisymmetric, and is the key actor in computing any observable. In particular, entanglement entropy on a bipartition $A \cup B$ is obtained by diagonalizing $\tilde{W}|_{A(B)}$, that is, restricting the indices of the Majorana fermions within either partition. If the eigenvalues of $\tilde{W}|_A$ are λ_k, then the entanglement entropy is given by

$$S = -\sum_k \left(\frac{1+\lambda_k}{2} \ln \frac{1+\lambda_k}{2} + \frac{1-\lambda_k}{2} \ln \frac{1-\lambda_k}{2} \right). \quad (B15)$$

4. Numerical implementation

The numerical implementation can be adapted to the protocol considered. For the quantum state diffusion, it is practical to divide the unitary step from the noise term $d\mathcal{Z}_t = -i\mathcal{H}dt + dT$. The Hamiltonian H can be stored and exponentiated only once, while the noise term dT is diagonal, with elements $dT_{ij} = \delta_{ij}[d\xi^i + \gamma dt(2\langle n_i \rangle - 1)]/2$ that needs to be computed repeatedly at each time step.

The resulting evolution then is

$$\tilde{\mathcal{U}}_{t+dt} = \mathcal{N} e^{2dT} e^{2i\mathcal{H}dt} \mathcal{U}_t, \qquad (B16)$$

where we have neglected higher order terms $O(d\xi dt)$ (Trotter approximation). The normalization $\mathcal{N}$ is unimportant, as Eq. (B16) is followed by a $\mathcal{QR}$ decomposition $\tilde{\mathcal{U}}_{t+dt} = \mathcal{Q}_{t+dt} \mathcal{R}_{t+dt}$, and by setting $\mathcal{U}_{t+dt} = \mathcal{Q}_{t+dt}$. As previously discussed, this condition guarantees the state is in the form of Eq. (B9) and the correlation function is obtained through Eq. (B11).

For the non-Hermitian quantum evolution, it is sufficient to exponentiate once the operator $d\mathcal{Z}_t = -i\mathcal{H}_{\text{eff}} dt$ and apply it subsequently to generate the evolution

$$\tilde{\mathcal{U}}_{t+dt} = \mathcal{N} e^{2i\mathcal{H}_{\text{eff}} dt} \mathcal{U}_t. \qquad (B17)$$

After each time step, the $\mathcal{QR}$ decomposition is implemented to normalize the state. In both situations, the entanglement entropy is computed as described in Appendix B 3.

[1] A. Polkovnikov, K. Sengupta, A. Silva, and M. Vengalattore, Colloquium: Nonequilibrium dynamics of closed interacting quantum systems, Rev. Mod. Phys. **83**, 863 (2011).

[2] L. D'Alessio, Y. Kafri, A. Polkovnikov, and M. Rigol, From quantum chaos and eigenstate thermalization to statistical mechanics and thermodynamics, Adv. Phys. **65**, 239 (2016).

[3] H. P. Breuer, and F. Petruccione, *The Theory of Open Quantum Systems* (Oxford University Press, Oxford, 2002).

[4] R. Nandkishore, and D. A. Huse, Many-body localization and thermalization in quantum statistical mechanics, Annu. Rev. Condens. Matter Phys. **6**, 15 (2015).

[5] D. Abanin, E. Altman, I. Bloch, and M. Serbyn, Colloquium: Many-body localization, thermalization, and entanglement, Rev. Mod. Phys. **91**, 021001 (2019).

[6] Y. Li, X. Chen, and M. P. A. Fisher, Quantum Zeno effect and the many-body entanglement transition, Phys. Rev. B **98**, 205136 (2018).

[7] M. J. Gullans and D. A. Huse, Dynamical Purification Phase Transition Induced by Quantum Measurements, Phys. Rev. X **10**, 041020 (2020).

[8] M. J. Gullans, and D. A. Huse, Scalable Probes of Measurement-Induced Criticality, Phys. Rev. Lett. **125**, 070606 (2020).

[9] Y. Li, X. Chen, and M. P. A. Fisher, Measurement-driven entanglement transition in hybrid quantum circuits, Phys. Rev. B **100**, 134306 (2019).

[10] Y. Li, X. Chen, A. W. W. Ludwig, and M. P. A. Fisher, Conformal invariance and quantum non-locality in hybrid quantum circuits, arXiv:2003.12721.

[11] A. Chan, R. M. Nandkishore, M. Pretko, and G. Smith, Unitary-projective entanglement dynamics, Phys. Rev. B **99**, 224307 (2019).

[12] A. Chan, R. M. Nandkishore, M. Pretko, and G. Smith, Measurement-induced criticality in random quantum circuits, Phys. Rev. B **101**, 104302 (2020).

[13] A. Zabalo, M. J. Gullans, J. H. Wilson, S. Gopalakrishnan, D. A. Huse, and J. H. Pixley, Critical properties of the measurement-induced transition in random quantum circuits, Phys. Rev. B **101**, 060301(R) (2020).

[14] J. Lopez-Piqueres, B. Ware, and R. Vasseur, Mean-field entanglement transitions in random tree tensor networks, Phys. Rev. B **102**, 064202 (2020).

[15] B. Skinner, J. Ruhman, and A. Nahum, Measurement-Induced Phase Transitions in the Dynamics of Entanglement, Phys. Rev. X **9**, 031009 (2019).

[16] A. Nahum, S. Roy, B. Skinner, and J. Ruhman, Measurement and entanglement phase transitions in all-to-all quantum circuits, on quantum trees, and in Landau-Ginsburg theory, PRX Quantum **2**, 010352 (2021).

[17] S. Choi, Y. Bao, X.-L. Qi, and E. Altman, Quantum Error Correction in Scrambling Dynamics and Measurement-Induced Phase Transition, Phys. Rev. Lett. **125**, 030505 (2020).

[18] Y. Bao, S. Choi, and E. Altman, Theory of the phase transition in random unitary circuits with measurements, Phys. Rev. B **101**, 104301 (2020).

[19] Y. Li, and M. P. A. Fisher, Statistical mechanics of quantum error-correcting codes, Phys. Rev. B **103**, 104306 (2021).

[20] R. Fan, S. Vijay, A. Vishwanath, and Y.-Z. You, Self-organized error correction in random unitary circuits with measurement, Phys. Rev. B **103**, 174309 (2021).

[21] M. Szyniszewski, A. Romito, and H. Schomerus, Entanglement transition from variable-strength weak measurements, Phys. Rev. B **100**, 064204 (2019).

[22] L. Zhang, J. A. Reyes, S. Kourtis, C. Chamon, E. R. Mucciolo, and A. E. Ruckenstein, Nonuniversal entanglement level statistics in projection-driven quantum circuits, Phys. Rev. B **101**, 235104 (2020).

[23] K. Snizhko, P. Kumar, and A. Romito, Quantum Zeno effect appears in stages, Phys. Rev. Research **2**, 033512 (2020).

[24] O. Shtanko, Y. A. Kharkov, L. P. García-Pintos, and A. V. Gorshkov, Classical models of entanglement in monitored random circuits, arXiv:2004.06736.

[25] O. Lunt, M. Szyniszewski, and A. Pal, Dimensional hybridity in measurement-induced criticality, arXiv:2012.03857.

[26] X. Turkeshi, R. Fazio, and M. Dalmonte, Measurement-induced criticality in $(2+1)$-dimensional hybrid quantum circuits, Phys. Rev. B **102**, 014315 (2020).

[27] C.-M. Jian, B. Bauer, A. Keselman, and A. W. W. Ludwig, Criticality and entanglement in non-unitary quantum circuits and tensor networks of non-interacting fermions, arXiv:2012.04666.

[28] S. Sang, Y. Li, T. Zhou, X. Chen, T. H. Hsieh, and M. P. A. Fisher, Entanglement negativity at measurement-induced criticality, arXiv:2012.00031.

[29] B. Shi, X. Dai, and Y.-M. Lu, Entanglement negativity at the critical point of measurement-driven transition, arXiv:2012.00040.

[30] M. Ippoliti and V. Khemani, Postselection-Free Entanglement Dynamics via Spacetime Duality, Phys. Rev. Lett. **126**, 060501 (2021).

[31] A. Lavasani, Y. Alavirad, and M. Barkeshli, Measurement-induced topological entanglement transitions in symmetric random quantum circuits, Nat. Phys. **17**, 342 (2021).

[32] A. Lavasani, Y. Alavirad, and M. Barkeshli, Topological order and criticality in (2+1)D monitored random quantum circuits, arXiv:2011.06595.

[33] S. Sang and T. H. Hsieh, Measurement protected quantum phases, arXiv:2004.09509.

[34] M. Ippoliti, M. J. Gullans, S. Gopalakrishnan, D. A. Huse, and V. Khemani, Entanglement Phase Transitions in Measurement-Only Dynamics, Phys. Rev. X **11**, 011030 (2021).

[35] N. Lang, and H. P. Büchler, Entanglement transition in the projective transverse field Ising model, Phys. Rev. B **102**, 094204 (2020).

[36] X. Turkeshi, Measurement-induced criticality as a data-structure transition, arXiv:2101.06245.

[37] Y. Fuji, and Y. Ashida, Measurement-induced quantum criticality under continuous monitoring, Phys. Rev. B **102**, 054302 (2020).

[38] D. Rossini and E. Vicari, Measurement-induced dynamics of many-body systems at quantum criticality, Phys. Rev. B **102**, 035119 (2020).

[39] O. Lunt and A. Pal, Measurement-induced entanglement transitions in many-body localized systems, Phys. Rev. Research **2**, 043072 (2020).

[40] S. Goto and I. Danshita, Measurement-induced transitions of the entanglement scaling law in ultracold gases with controllable dissipation, Phys. Rev. A **102**, 033316 (2020).

[41] Q. Tang and W. Zhu, Measurement-induced phase transition: A case study in the nonintegrable model by density-matrix renormalization group calculations, Phys. Rev. Research **2**, 013022 (2020).

[42] X. Cao, A. Tilloy, and A. De Luca, Entanglement in a fermion chain under continuous monitoring, SciPost Phys. **7**, 024 (2019).

[43] L. Fidkowski, J. Haah, and M. B. Hastings, How dynamical quantum memories forget, Quantum **5**, 382 (2021).

[44] O. Alberton, M. Buchhold, and S. Diehl, Trajectory Dependent Entanglement Transition in a Free Fermion chain—From Extended Criticality to Area Law, Phys. Rev. Lett. **126**, 170602 (2021).

[45] X. Chen, Y. Li, M. P. A. Fisher, and A. Lucas, Emergent conformal symmetry in nonunitary random dynamics of free fermions, Phys. Rev. Research **2**, 033017 (2020).

[46] Q. Tang, X. Chen, and W. Zhu, Quantum criticality in nonunitary dynamics of $(2+1)$-dimensional free fermions, Phys. Rev. B **103**, 174303 (2021).

[47] A. Nahum and B. Skinner, Entanglement and dynamics of diffusion-annihilation processes with Majorana defects, Phys. Rev. Research **2**, 023288 (2020).

[48] Y. Bao, S. Choi, and E. Altman, Symmetry enriched phases of quantum circuits, arXiv:2102.09164.

[49] A. Biella and M. Schiró, Many-body quantum Zeno effect and measurement-induced subradiance transition, arXiv:2011.11620.

[50] S. Gopalakrishnan and M. J. Gullans, Entanglement and Purification Transitions in Non-Hermitian Quantum Mechanics, Phys. Rev. Lett. **126**, 170503 (2021).

[51] S.-K. Jian, Z.-C. Yang, Z. Bi, and X. Chen, Yang-Lee edge singularity triggered entanglement transition, arXiv:2101.04115.

[52] M. Buchhold, Y. Minoguchi, A. Altland, and S. Diehl, Effective theory for the measurement-induced phase transition of Dirac fermions, arXiv:2102.08381.

[53] N. Gisin and I. C. Percival, The quantum-state diffusion model applied to open systems, J. Phys. A: Math. Gen. **25**, 5677 (1992).

[54] T. A. Brun, A simple model of quantum trajectories, Am. J. Phys. **70**, 719 (2002).

[55] C. W. Gardiner and P. Zoller, *Quantum Noise* (Springer-Verlag, Berlin/Heidelberg, 2000).

[56] H. M. Wiseman, and G. J. Milburn, Quantum theory of field-quadrature measurements, Phys. Rev. A **47**, 642 (1993).

[57] D. Yang, C. Laflamme, D. V. Vasilyev, M. A. Baranov, and P. Zoller, Theory of a Quantum Scanning Microscope for Cold Atoms, Phys. Rev. Lett. **120**, 133601 (2018).

[58] R. Frassek, C. Giardiná, and J. Kurchan, Duality in quantum transport models, SciPost Phys. **10**, 135 (2021).

[59] P. Calabrese and J. Cardy, Entanglement entropy and quantum field theory, J. Stat. Mech. (2004) P06002.

[60] L. Amico, R. Fazio, A. Osterloh, and V. Vedral, Entanglement in many-body systems, Rev. Mod. Phys. **80**, 517 (2008).

[61] R. Horodecki, P. Horodecki, M. Horodecki, and K. Horodecki, Quantum entanglement, Rev. Mod. Phys. **81**, 865 (2009).

[62] N. Laflorencie, Quantum entanglement in condensed matter systems, Phys. Rep. **646**, 1 (2016).

[63] V. Alba, and F. Carollo, Spreading of correlations in Markovian open quantum systems, Phys. Rev. B **103**, L020302 (2021).

[64] M. B. Plenio and P. L. Knight, The quantum-jump approach to dissipative dynamics in quantum optics, Rev. Mod. Phys. **70**, 101 (1998).

[65] J. M. Hickey, S. Genway, I. Lesanovsky, and J. P. Garrahan, Time-integrated observables as order parameters for full counting statistics transitions in closed quantum systems, Phys. Rev. B **87**, 184303 (2013).

[66] T. E. Lee and C.-K. Chan, Heralded Magnetism in Non-Hermitian Atomic Systems, Phys. Rev. X **4**, 041001 (2014).

[67] P. Calabrese and J. Cardy, Entanglement entropy and conformal field theory, J. Phys. A: Math. Theor. **42**, 504005 (2009).

[68] D. Bianchini, O. Castro-Alvaredo, B. Doyon, E. Levi, and F. Ravanini, Entanglement entropy of non-unitary conformal field theory, J. Phys. A: Math. Theor. **48**, 04FT01 (2014).

[69] R. Couvreur, J. L. Jacobsen, and H. Saleur, Entanglement in Nonunitary Quantum Critical Spin Chains, Phys. Rev. Lett. **119**, 040601 (2017).

[70] K. Jacobs and D. A. Steck, A straightforward introduction to continuous quantum measurement, Contemp. Phys. **47**, 279 (2006).

[71] H. M. Wiseman and G. J. Milburn, *Quantum Measurement and Control* (Cambridge University Press, Cambridge, UK, 2009).

[72] G. B. Mbeng, A. Russomanno, and G. E. Santoro, The Quantum Ising Chain for Beginners, arXiv:2009.09208.